Endothelial sphingosine 1-phosphate receptors promote vascular normalization and antitumor therapy

Andreane Cartier[a,b], Tani Leigh[b], Catherine H. Liu[c], and Timothy Hla[a,b,1]

[a]Vascular Biology Program, Boston Children's Hospital, Boston, MA 02115; [b]Department of Surgery, Harvard Medical School, Boston, MA 02115; and [c]Department of Pathology and Laboratory Medicine, Weill Cornell Medicine, New York, NY 10065

Edited by Kari Alitalo, University of Helsinki, Helsinki, Finland, and approved December 31, 2019 (received for review April 12, 2019)

Sphingosine 1-phosphate receptor-1 (S1PR1) is essential for embryonic vascular development and maturation. In the adult, it is a key regulator of vascular barrier function and inflammatory processes. Its roles in tumor angiogenesis, tumor growth, and metastasis are not well understood. In this paper, we show that S1PR1 is expressed and active in tumor vessels. Murine tumor vessels that lack S1PR1 in the vascular endothelium (*S1pr1* ECKO) show excessive vascular sprouting and branching, decreased barrier function, and poor perfusion accompanied by loose attachment of pericytes. Compound knockout of *S1pr1*, 2, and 3 genes further exacerbated these phenotypes, suggesting compensatory function of endothelial S1PR2 and 3 in the absence of S1PR1. On the other hand, tumor vessels with high expression of S1PR1 (*S1pr1* ECTG) show less branching, tortuosity, and enhanced pericyte coverage. Larger tumors and enhanced lung metastasis were seen in *S1pr1* ECKO, whereas *S1pr1* ECTG showed smaller tumors and reduced metastasis. Furthermore, antitumor activity of a chemotherapeutic agent (doxorubicin) and immune checkpoint inhibitor blocker (anti-PD-1 antibody) were more effective in *S1pr1* ECTG than in the wild-type counterparts. These data suggest that tumor endothelial S1PR1 induces vascular normalization and influences tumor growth and metastasis, thus enhancing antitumor therapies in mouse models. Strategies to enhance S1PR1 signaling in tumor vessels may be an important adjunct to standard cancer therapy of solid tumors.

angiogenesis | cancer | immunotherapy | sphingosine 1-phosphate | G protein-coupled receptor

Sphingosine 1-phosphate (S1P), a lysophospholipid found in blood and lymph, regulates cell survival, migration, immune cell trafficking, angiogenesis, and vascular barrier function (1). S1P binds to the family of G protein-coupled sphingosine 1-phosphate receptors 1 to 5 (S1PR1 to 5) which are expressed on most cells (2). The prototypical S1PR1, which is abundantly expressed in vascular endothelial cells (ECs), is required for embryonic vascular development and maturation (3, 4). S1PR1 inhibits VEGF-induced vascular sprouting (5) by promoting interactions between VE-cadherin and VEGFR2 that suppress VEGF signaling (6). However, S1PR1 function is compensated by other S1PRs that are expressed in ECs, albeit at lower levels. For example, S1PR2 and S1PR3, which are both capable of signaling via the Gi pathway, function redundantly as S1PR1 in embryonic vascular development (7). Mice that lack S1PR1, 2, and 3 exhibit early embryonic lethality similar to global (8) or red blood cell–specific (9) sphingosine kinase (SPHK)-1 and -2 double-knockout mice that lack circulatory S1P. These findings support the notion that coordinated signaling of VEGF-A via its receptor tyrosine kinases and plasma S1P via EC G protein-coupled S1PRs is fundamental for the development of a normal primary vascular network.

Tumor progression requires new vessel growth, a phenomenon termed tumor angiogenesis. This is achieved by the production of angiogenic factors which activate endothelial cells from preexisting blood vessels to undergo angiogenesis (10). For example, angiogenic stimulators such as VEGF-A are released by tumor cells to induce angiogenesis and tumor growth (11). Angiogenesis is also associated with spreading of tumors to metastatic sites. Tumor vessels, characterized by abnormal morphology, are highly dysfunctional in their barrier and transport properties (12). Strategies to induce phenotypic change in tumor vessels to resemble normal vessels, termed vascular normalization, have been attempted (12–14). Indeed, anti-VEGF antibodies induce vascular normalization in preclinical models and in the clinic, which may in part explain their efficacy in the treatment of metastatic cancer. After anti-VEGF treatment, tumor vessels show increased perfusion and efficacy of antitumor chemotherapies. However, preclinical studies have shown that a precise time window of administration is needed for the efficacy of antiangiogenic therapies, as prolonged antiangiogenic treatment can lead to excessive pruning, hypoxia, activation of alternative proangiogenic pathways, and the development of resistance (15).

Even though S1P signaling via endothelial S1PRs is a central player in vascular development, the role of the S1P signaling axis in tumor angiogenesis and progression is not clear. Early studies showed that S1PR1 is expressed in tumor vessels and down-regulation of its expression with 3′UTR-targeted multiplex small interfering RNAs (siRNAs) suppressed tumor growth in mouse models (16). Moreover, administration of FTY720, a prodrug that is phosphorylated and binds to four out of five S1P receptors, suppressed tumor growth and metastasis in mouse models (17, 18). Application of VEGF pathway inhibitors together with S1PR-targeted small molecules achieved better inhibition of tumor angiogenesis (19). However, precise roles of endothelial S1PR

Significance

Tumor progression is dependent on angiogenesis, which supplies nutrients and enables gas exchange and metastatic dissemination. However, tumor vessels are dysfunctional and immature, which hinders the effectiveness of various therapeutics. Sphingosine 1-phosphate receptors in endothelial cells are essential for developmental angiogenesis and physiological functions such as the maintenance of the vascular barrier and vascular tone. This study shows that endothelial sphingosine 1-phosphate receptors determine the tumor vascular phenotype and maturation and that function of S1P receptor-1 is needed for tumor vascular normalization, which allows better blood circulation and enhances antitumor therapeutic efficacy in mouse models.

Author contributions: A.C. and T.H. designed research; A.C., T.L., and C.H.L. performed research; C.H.L. contributed new reagents/analytic tools; A.C. and T.H. analyzed data; and A.C. and T.H. wrote the paper.

Competing interest statement: T.H. discloses that he received research funding from ONO Pharmaceutical Corporation, consulted for Astellas, Steptoe and Johnson, Gerson Lehrman Group Council, Janssen Research & Development, LLC, and Sun Pharma advanced research group (SPARC) and is an inventor on patents/patent applications on ApoM+HDL, S1P chaperones, and S1P receptor antagonists.

This article is a PNAS Direct Submission.

[1]To whom correspondence may be addressed. Email: timothy.hla@childrens.harvard.edu.

This article contains supporting information online at https://www.pnas.org/lookup/suppl/doi:10.1073/pnas.1906246117/-/DCSupplemental.

First published January 27, 2020.

subtypes in tumor angiogenesis, progression, and metastasis have not been analyzed in preclinical models. We systematically studied mouse genetic models in which S1PRs have been modified either alone or in combination and studied tumor vascular phenotypes in syngeneic lung cancer, melanoma, and breast cancer models. We show that endothelial S1PRs are key regulators of vascular normalization and that stimulation of this pathway enhances chemotherapeutic and immunotherapeutic efficacy.

Results

S1PR1 Regulates Tumor Vascular Phenotype and Mural Cell Coverage of Tumor Vessels. S1PR1 is expressed in angiogenic vessels of tumors grown subcutaneously (s.c.) in mice (16). In order to determine whether S1PR1 is actively signaling in angiogenic endothelial cells, we used a mouse model referred to as S1PR1-GFP signaling mice that allows visualization of the β-arrestin recruitment to S1PR1 (20). We injected Lewis lung carcinoma cells (LLCs) s.c. in S1PR1-GFP signaling mice as well as H2B-GFP control mice and analyzed the resected tumor sections by confocal fluorescence microscopy. GFP positivity was observed in tumor vessel-like structures in S1PR1-GFP signaling mice but not in the control H2B-GFP. The quantification of several sections from three S1PR1-GFP tumors stained with cluster of differentiation 31 (CD31) showed an average of 50 ± 20 pixels of GFP colocalized with CD31, while sections from two H2B-GFP tumors showed none. Moreover, the majority of GFP^+ cells were colocalized with $CD31^+$ cells but not with α-smooth muscle actin $(\alpha\text{-SMA})^+$ cells (Fig. 1 *A*–*D*). Non-$CD31^+$ GFP^+ cells are likely intratumoral hematopoietic cells. These data suggest that S1PR1 signaling is active in endothelial cells of angiogenic tumors.

To assess the functional role of S1PR1 in tumor angiogenesis, we used a mouse model in which *S1pr1* is deleted specifically in endothelial cells by tamoxifen-activated Cre recombinase (*S1pr1*$^{flox/flox}$ *Cdh5 Cre-ER*^{T2}), which is referred to as *S1pr1* ECKO (5, 21–23). Tumors grown in *S1pr1* ECKO mice were almost 2 times bigger than the tumors grown in control mice (Fig. 1*E*). The differences between wet and dry tumor mass between the *S1pr1* ECKO and control mice were similar (*SI Appendix*, Fig. S1*A*), suggesting that edema in the tumor cannot account for the increase. Histological analysis did not reveal marked changes in extracellular matrix accumulation or fibrosis (*SI Appendix*, Fig. S1*B*). These data suggest that increased tumor cell proliferation and/or recruitment of host-derived cells may lead to increased tumor growth in the absence of endothelial S1PR1.

To determine the functional role of S1PR1 in tumor angiogenesis, vascular density and morphology were assessed in tumor sections stained for CD31 and analyzed by light (*SI Appendix*, Fig. S1*C*) and confocal fluorescence microscopy (Fig. 1*F*) followed by quantitative image analysis (*SI Appendix*, Fig. S1*D*). Tumor vessels in *S1pr1* ECKO mice show higher vascular density with increased vascular sprouts and branches (Fig. 1 *G* and *H*). These data indicate that S1PR1 is present and active in tumor vascular endothelial cells and suppresses hypersprouting of intratumoral vessels.

During embryonic development, S1PR1 expression on endothelial cells is important for vascular stabilization and mural cell recruitment (4). Sections from tumors grown in *S1pr1* ECKO and control animals were assessed for mural cell coverage. Immunohistochemical staining with α-SMA antibody shows that tumor vessels from *S1pr1* ECKO are deficient in SMA-positive cell coverage by immunofluorescence (IF) confocal microscopy (Fig. 1*I*) and immunohistochemistry (IHC) (*SI Appendix*, Fig. S1*E*). On the other hand, chondroitin sulfate proteoglycan $(NG2^+)$ pericytes were similar in number in both wild type (WT) and *S1pr1* ECKO tumor vessels (Fig. 1 *K* and *L*). However, pericyte attachment to the endothelial cells in the tumor vessels from *S1pr1* ECKO mice appeared loose, with pericytes weakly tethered to the endothelial cell layer, which is in sharp contrast to the WT counterparts. The lack of $\alpha\text{-SMA}^+$ mural cell coverage and loose association of $NG2^+$ pericytes may in part explain the biological basis of the altered vascular morphology seen in *S1pr1* ECKO tumor vessels.

Tumors in *S1pr1* ECKO Mice Show Increased Vascular Permeability and Metastatic Potential. Since tumor vessels from *S1pr1* ECKO mice showed deficient maturation, we characterized their vascular barrier properties. We performed intravenous (i.v.) injection of high molecular weight fluorescein isothiocyanate conjugated–dextran (2,000 kDa) and tetramethylrhodamine-dextran (70 kDa) and assessed vascular leak in tumor vessels (Fig. 2*A*). Quantification of tissue sections from tumors from *S1pr1* ECKO revealed increased leakage of the 70 kDa dextran in the proximity of the vessels (Fig. 2*B*) while the 2000 kDa dextran was mostly intraluminal. Higher-magnification images are shown in *SI Appendix*, Fig. S2*A*.

Since vascular leakage can lead to tissue perfusion defects and hypoxia (24), we used the oxygen-sensitive probe (Hypoxyprobe-1) to determine the hypoxic status of tumors in WT and *S1pr1* ECKO mice (25). As shown in Fig. 2*C*, quantification of the hypoxic index of the *S1pr1* ECKO tumor section stained for CD31 and Hypoxyprobe-1 antibody (*SI Appendix*, Fig. S2*B*) trended toward an increase, even though the difference was statistically not significant, suggesting a minor and heterogeneous change in tumor oxygenation.

Lungs from mice injected with 2,000 and 70 kDa dextran were sectioned, and extravasation of 70 kDa dextran was also observed (Fig. 2*D*). i.v. tail vein injection of B16F10 melanoma cells into WT and *S1pr1* ECKO mice, which results in lung metastasis, showed markedly increased metastatic foci in the lungs of the mice that lacked endothelial S1PR1 (Fig. 2 *E* and *F*), suggesting that aforementioned vascular defects contributed to lung colonization of circulating tumor cells and metastasis.

Taken together, these data show that S1PR1 expressed on endothelial cells regulates tumor angiogenesis, vessel maturation, vascular permeability, and tumor perfusion, thus influencing primary tumor growth and metastatic potential in mouse models.

Endothelial Cell S1PR1 Alters the Immune Cell Repertoire in the Tumor Microenvironment. The tumor microenvironment (TME), which comprises several innate and adaptive immune cell types, among other nonimmune cell types, plays an important role in tumorigenesis and antitumor immunity (26–29). We assessed if the endothelial S1PR1 function could influence the immune cell populations present in the TME of the s.c. LLC tumors. The harvested tumors were digested, and the single-cell suspensions were analyzed by flow cytometry. We specifically focused on intratumoral T cells, M1- and M2- polarized macrophages, dendritic cells (DCs), myeloid-derived suppressor cells (MDSCs), and natural killer cells (NKs). As presented in Fig. 3, endothelial loss of S1PR1 led to a reduction in CD45+ cells, M1 and M2 macrophages, and DCs, while $CD3^+$ T cells, MDSCs, and NK cells in the tumors were not significantly altered. These data suggest that endothelial S1PR1 maintains the myeloid populations in the TME, which influences tumor growth and metastasis.

Redundant Functions of S1PR2 and 3 in the Regulation of the Tumor Vascular Phenotypes, Tumor Growth, and Metastasis. Endothelial cells express S1PR2 and S1PR3 in addition to S1PR1 (30). While S1PR1 and S1PR2 induce opposing cellular effects, for example, in barrier function, S1PR2 can activate redundant signaling pathways in the absence of S1PR1 (31–33). In addition, both S1PR2 and S1PR3 are capable of signaling redundantly as S1PR1, for example, via the G_i pathway (34–37). The roles of these receptors in tumor angiogenesis have not been examined.

We recently developed a conditional mutant allele for *S1pr2* and developed a mouse model for *S1pr2* ECKO using the tamoxifen-inducible Cdh5-Cre driver (38). Using this mouse model

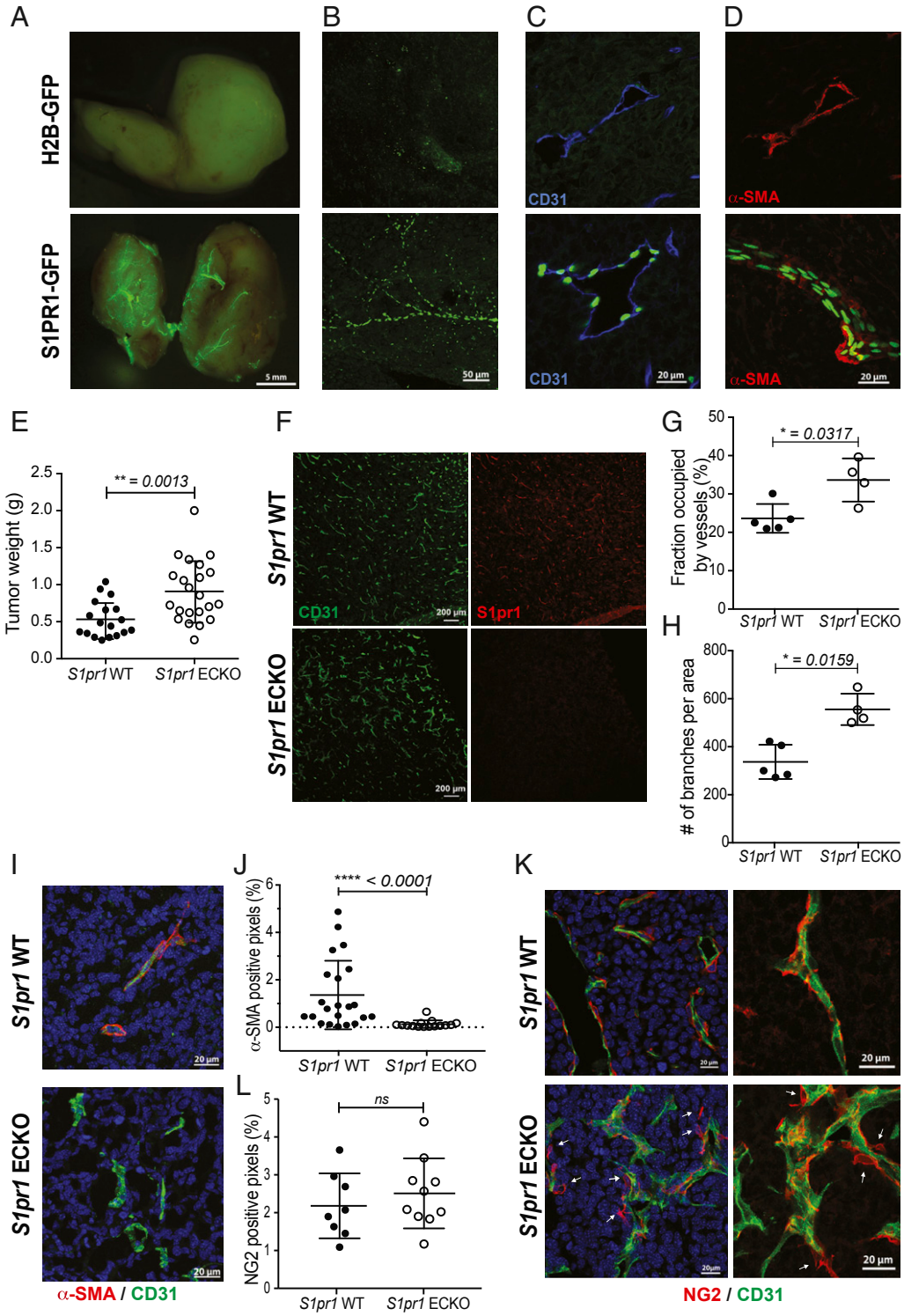

Fig. 1. Loss of EC-specific S1PR1 induces tumor growth and angiogenesis and impairs mural cell coverage. (*A*–*D*) s.c. LLC tumors grown in S1PR1-GFP and H2B-GFP control mice show a positive GFP signal in vascular structures, while the tumors grown in the control mice show no GFP-positive vascular structures. Whole-mount fluorescence imaging (*A*) and two-photon (*B*) and confocal (*C* and *D*) microscopy of 35 μm tumor sections stained with CD31 and α-SMA. n = 3 independent experiments. (*E*) Weight of s.c. LLC tumors grown in control *S1pr1* WT and ECKO mice. $n = 6$ independent experiments containing three or four mice per group, expressed as a mean of two tumors per animal ± SD. (*F*) IF of 35 μm sections of tumor, frozen in OCT and stained with S1PR1 and CD31 antibodies, shows extensive deletion of S1PR1 signal in endothelial cells by confocal microscopy. (*G* and *H*) Quantification of vascular density and branching from immunofluorescence images (n = 4 to 5) from tumors grown in control *S1pr1* WT and ECKO mice. Data are expressed as mean ± SD. (*I*) IF of tumor sections from *S1pr1* WT and ECKO mice and stained with α-SMA antibody and CD31. (*J*) Quantification of α-SMA positive pixels from confocal images (n = 15 to 22) of sections from tumors grown in control *S1pr1* WT and ECKO mice. (*K*) Low- and high-magnification confocal images of frozen OCT tumor sections stained with CD31 and pericyte marker NG2. Arrows indicate areas of loose pericyte coverage of the endothelium. (*L*) Quantification of total NG2-positive signal from confocal images ($n = 8$ to 10). Data are expressed as mean ± SD. P values were determined by a two-tailed unpaired Mann–Whitney U test comparing control *S1pr1* WT and *S1pr1* ECKO mice. ns, nonsignificant; $^*P \leq 0.05$, $^{**}P \leq 0.01$, $^{****}P \leq 0.0001$.

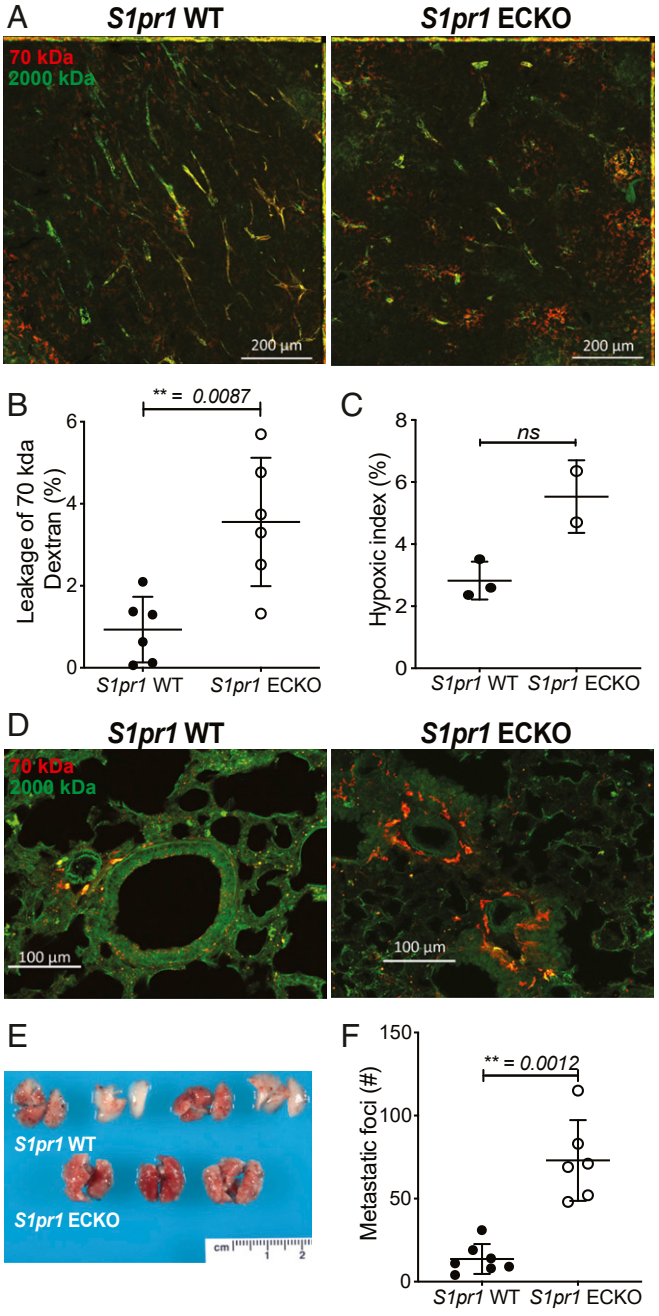

Fig. 2. EC-specific S1PR1-deficient tumor vessels show increased leakage and metastasis. (*A*) Confocal images of 35 µm tumor sections grown in *S1pr1* WT and ECKO mice, i.v. injected with 2,000 kDa (fluorescein, green) and 70 kDa (tetramethylrhodamine-conjugated dextran [TMR], red) dextran (n = 6 per group). (*B*) Quantification of extravasated 70 kDa dextran from confocal images (n = 6). Data are expressed as mean ± SD. *P* values were determined by a two-tailed unpaired Mann–Whitney *U* test comparing control *S1pr1* WT and *S1pr1* ECKO mice. (*C*) Quantification of Hypoxyprobe-1 staining images from a tumor grown in *S1pr1* WT and ECKO mice (n = 3). *P* values were determined by a two-tailed unpaired *t* test with Welch's correction comparing control *S1pr1* WT and *S1pr1* ECKO mice. (*D*) Confocal images of lung sections from tumor-bearing *S1pr1* WT and ECKO mice that were injected i.v. with 2,000 kDa (fluorescein, green) and 70 kDa (TMR, red) dextran (n = 6 per group). (*E*) Lung colonization of B16F10 cells injected i.v. in *S1pr1* WT and ECKO mice. The image is representative of three independent experiments. (*F*) Quantification of metastatic foci. Data are expressed as mean ± SD. *P* values were determined by a two-tailed unpaired Mann–Whitney *U* test comparing control and *S1pr1* ECKO mice. ns, nonsignificant; $^{**}P \leq 0.01$.

with LLC tumors, tumor angiogenesis and vascular phenotypes were analyzed. As shown in Fig. 4*A*, tumors grown in *S1pr2* ECKO mice were significantly smaller than those in the WT counterparts. Tumor vasculature showed no significant changes in permeability to i.v. injected 70 kDa fluorescent dextran (*SI Appendix*, Fig. S3 *A* and *B*). However, increased pericyte coverage was seen (Fig. 4 *B* and *C*). Moreover, i.v.-injected B16F10 melanoma cells showed decreased metastatic potential in the lungs of *S1pr2* ECKO (Fig. 4 *D* and *E*). These results reveal the opposing functions of S1PR1 and S1PR2 in tumor vascular phenotype regulation.

When compound *S1pr1*, *S1pr2* ECKO mice were analyzed, s.c. LLC tumors were similar in size (Fig. 4*F*), and α-SMA$^+$ and NG2$^+$ mural cells' recruitment to tumor vessels was not different from the control counterparts (*SI Appendix*, Fig. S4 *A* and *B*). Tumor vascular phenotype showed modest hypersprouting, suggesting that the effects of *S1pr1* ECKO were neutralized by the lack of S1PR2, which mediates opposite endothelial phenotypic effects. Additionally, the percentages of α-SMA$^+$-CD31$^+$ and NG2$^+$-CD31$^+$ double signal were similar in both *S1pr1*, *S1pr2* WT and ECKO mice (*SI Appendix*, Fig. S4 *C* and *D*).

We next examined the redundant role of S1PR3 in tumor angiogenesis. When *S1pr3*$^{-/-}$ mice (7) were compared with compound *S1pr1* ECKO *S1pr3*$^{-/-}$ mice, tumor growth (Fig. 4*G*), vascular density (*SI Appendix*, Fig. S5 *A* and *B*), and the recruitment of α-SMA$^+$ and NG2$^+$ mural cells to tumor vessels largely resembled those of *S1pr1* ECKO mice (*SI Appendix*, Fig. S5 *I* and *J*). However, compound triple KO of *S1pr1* and *S1pr2* ECKO in *S1pr3*$^{-/-}$ background showed a marked increase in tumor growth (Fig. 4*H*), vascular hypersprouting, hyperbranching, and mural cell disengagement phenotypes (Fig. 4*I*). Histological analysis by hematoxylin and eosin (H&E) and Masson's trichrome staining (*SI Appendix*, Fig. S6 *A* and *B*) shows that compound deletion of S1pr1, 2, and 3 strongly affects the tumor morphology. These data suggest that S1PR3 functions are redundant to S1PR1 in suppressing endothelial hypersprouting as well as properties of highly abnormal vascular phenotypes. Together, these findings support the redundant functions of S1PR2 and S1PR3, which compensate the function of attenuated S1PR1.

Overexpression of EC-Specific S1PR1 Enhances Mural Cell Coverage, and Reduces Tumor Growth, Vascular Leakage, and Metastasis. Due to the prominent role of endothelial S1PR1 in tumor vasculature, growth, and metastatic potential, we next analyzed the inducible S1PR1 endothelial-specific transgenic mice (*S1pr1*$^{flox/stop/flox}$ *Cdh5 Cre-ER*^{T2}) (ECTG) (5, 21). s.c. LLC tumor size was smaller in *S1pr1* ECTG mice (Fig. 5*A*), while intratumoral edema was not affected (*SI Appendix*, Fig. S7*A*), and histological analysis did not reveal marked changes in extracellular matrix accumulation or fibrosis (*SI Appendix*, Fig. S7*B*). Overexpression of S1PR1 in tumor vessels (Fig. 5*B*) tended to have less vascular branches and sprouts characterized by more linear and less tortuous vascular morphology (*SI Appendix*, Fig. S7 *C*–*E*), which is in contrast to the *S1pr1* ECKO counterparts described above.

Furthermore, *S1pr1* ECTG tumor vessels contained higher NG2$^+$ mural cells and trended toward an increase in SMA$^+$ mural cells (Fig. 5 *C*–*E*). Tumor vascular leakage of intravenously injected 70 kDa dextran trended toward being less than the controls but did not reach statistical significance (Fig. 5 *F* and *G*). Higher-magnification images are shown in *SI Appendix*, Fig. S7*F*. In contrast, the hypoxic index in the tumors was markedly reduced (Fig. 5*H*). i.v.-injected B16F10 melanoma cells also trended toward fewer metastatic foci in the lung (P = 0.0515) (Fig. 5 *I* and *J*). Together, these data suggest that increased S1PR1 expression in endothelial cells promotes tumor vascular normalization and suppresses metastatic potential. While loss of S1PR1 in EC reduced the myeloid cell population in the tumor microenvironment, immune cell populations in the *S1pr1* ECTG were not significantly different from those of the WT counterparts,

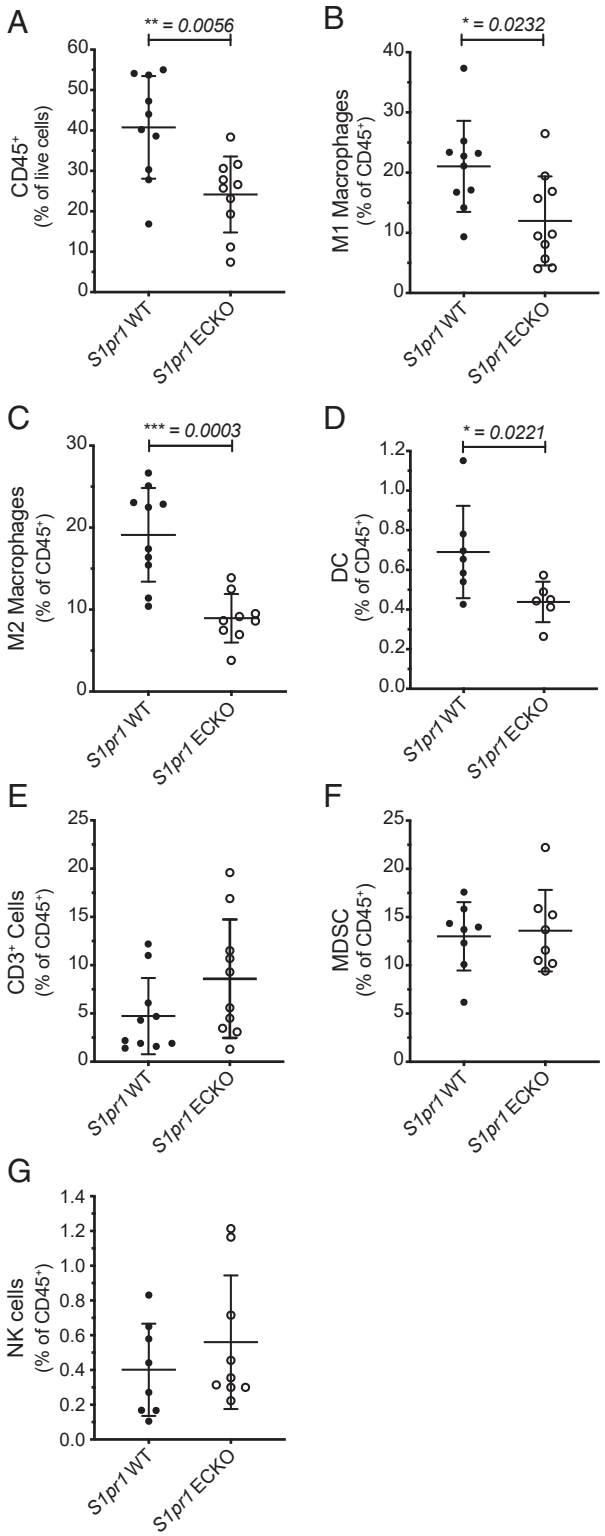

Fig. 3. Loss of EC-specific S1PR1 modifies the immune cell populations in the tumor microenvironment. Immune profile of LLC tumors grown in *S1pr1* WT and ECKO mice. Percentages of CD45$^+$(*A*), macrophages M1 (CD45$^+$, CD3$^-$, CD11b$^+$, MHCII^{hi}) (*B*) and M2 (CD45$^+$, CD3$^-$, CD11b$^+$, MHCII^{low}) (*C*), DCs (CD45$^+$, CD3$^-$, CD11c$^+$, CD11b$^-$) (*D*), CD3$^+$ cells (CD45$^+$, CD3$^+$) (*E*), MDSCs (CD45$^+$, CD3$^-$, CD11b$^+$, Ly6C$^+$/Ly6G$^+$) (*F*), and NK cells (CD45$^+$, CD3$^-$, CD49b$^+$) (*G*). $n = 4$ independent experiments, each containing two to four mice per group. *P* values were determined by a two-tailed unpaired Mann–Whitney *U* test comparing control and *S1pr1* ECKO mice. $*P \le 0.05$, $**P \le 0.01$, $***P \le 0.001$.

presumably because normal levels of S1PR1 are sufficient (*SI Appendix*, Fig. S8).

Overexpression of S1PR1 in Endothelial Cells Enhances the Efficacy of Antitumor Therapies. Doxorubicin is a widely used chemotherapeutic agent for the treatment of a plethora of cancers, but chronic or high doses exhibit adverse effects such as cardiotoxicity (39–41). As normalization of tumor vessels was shown to enhance antitumor therapies (12–15, 42), we combined the overexpression of S1PR1 in EC with doxorubicin treatments. We injected 5 mg/kg of doxorubicin into tumor-bearing WT and *S1pr1* ECTG mice every other day, starting at day 8 after injection of the LLCs. As expected, doxorubicin treatment reduced the growth of the tumors in both cohorts of mice. However, the tumors grown in the *S1pr1* ECTG mice and treated with doxorubicin exhibited the largest delay in growth (Fig. 6 *A*–*C*). Tumor immunotherapy with checkpoint inhibitors is also an emerging antitumor therapeutic strategy in melanomas and kidney and non-small-cell lung cancer (43). We chose the syngeneic murine breast adenocarcinoma cell line E0771 (44), which has shown sensitivity to anti-PD-1 antibody treatment in orthotopic tumor models in mice (45–47). Immunofluorescence staining of tumor sections shows that the vasculature in orthotopic E0771 tumors in WT and *S1pr1* ECTG mice exhibits high S1PR1 expression (Fig. 6*D*). While α-SMA staining was similar for both cohorts, the NG2$^+$ mural cell population was enhanced in the *S1pr1* ECTG mice, as it was observed with the LLC tumor grown in S1pr1 WT and ECTG. Overexpression of S1PR1 in EC reduced tumor growth in mice treated with saline, as was observed with s.c. LLC tumors. However, when tumor-bearing mice were treated with anti-PD-1 antibody, marked potency of the checkpoint inhibitor on tumor growth was seen in mice that expressed more S1PR1 in the tumor endothelium compared to their WT S1PR1 counterparts (Fig. 6 *E* and *F*). These data suggest that S1PR1-induced tumor vascular normalization enhances both the chemotherapeutic efficiency and immunotherapeutic efficiency of antitumor agents.

Discussion

The S1P signaling axis via the endothelial S1PRs represents a major regulatory system for vascular maturation during development (7). Balanced signaling between angiogenic growth factors, such as VEGF, which signals via receptor tyrosine kinases, and S1PRs, which are GPCRs, is essential for normal vascular development (48). In the adult, endothelial S1PR signaling regulates vascular barrier function, tone, and inflammatory processes. Since tumor angiogenesis occurs postnatally, we studied the role of the endothelial cell S1PR signaling axis in mouse models of tumor angiogenesis, progression, and metastasis.

A principle finding of our work is that the level of S1PR expression in the tumor endothelium determines key aspects of the tumor vascular phenotype. These include endothelial sprouting, branching phenotypes, and the barrier function. The lack of endothelial S1PR1 promoted excessive vascular leakage, as well as markedly increased vascular sprouting and branching. We predict that attenuated S1PR1 function in the tumor endothelium would lead to decreased access of blood-borne cells and substances to the tumor parenchyma. Opposite phenotypes were seen by overexpression of endothelial S1PR1. Our results suggest that S1PR1-regulated events in the newly formed tumor vessels are important in determining their normalization status.

We also show that attenuated endothelial S1PR1 function led to increased tumor growth, whereas S1PR1 overexpression led to smaller tumors. Intratumoral edema is unable to account for the changes in tumor size. However, we observe a marked diminution of various myeloid populations in the TME of *S1pr1* ECKO mice. In particular, both DCs and M1- and M2-polarized macrophages are reduced. Macrophage populations, in particular M1-polarized macrophages and MDSCs, are known to suppress tumor

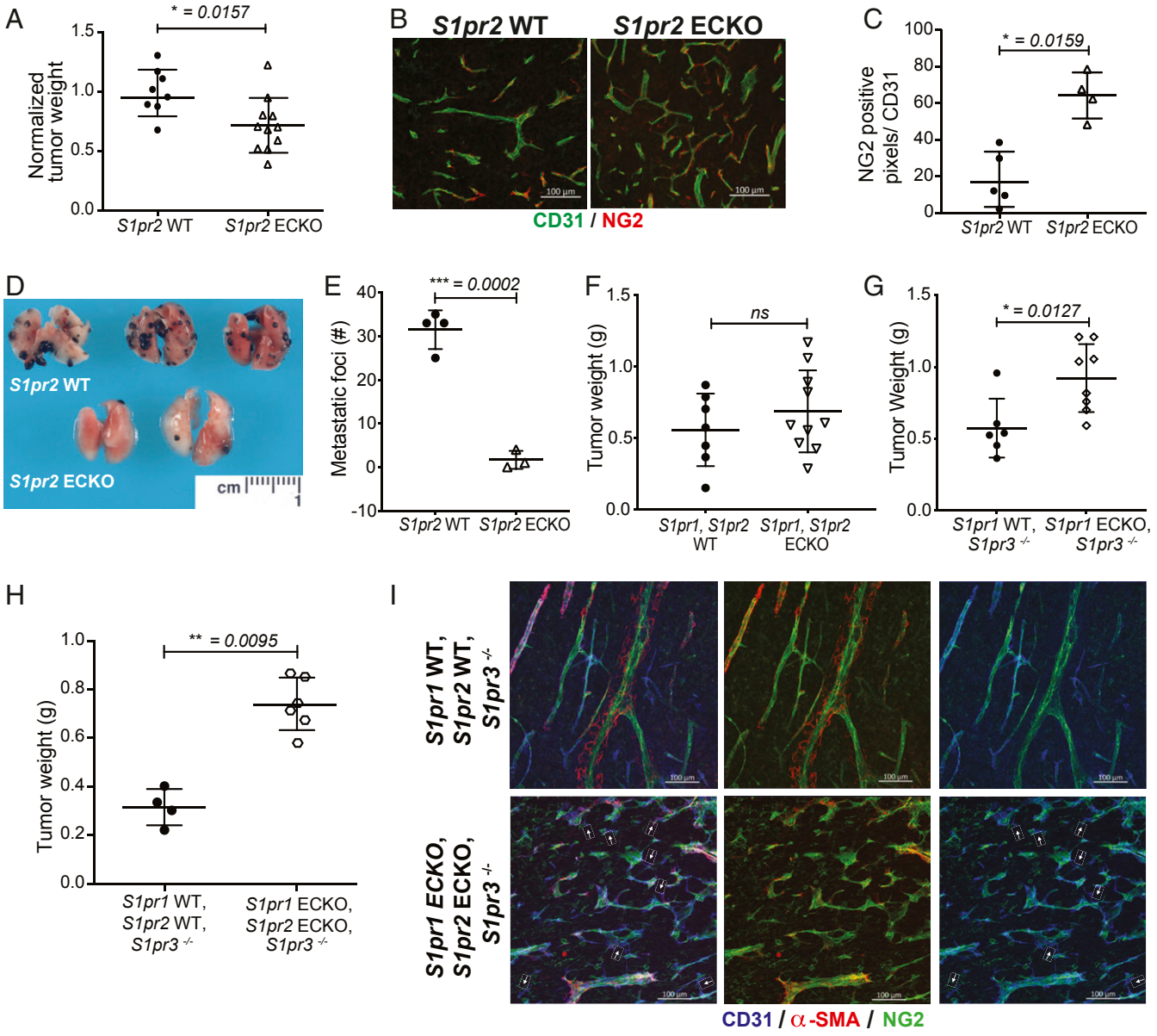

Fig. 4. Compound endothelial-specific deletion of *S1pr1* and *S1pr2* in *S1pr3*$^{-/-}$ background induces tumor growth and severe vascular disorganization. (*A*) Whole-tumor weight of s.c. LLC tumors grown in *S1pr2* WT and ECKO mice. $n = 3$ independent experiments containing three or four mice per group, expressed as a mean of two tumors per animal ± SD. (*B*) Confocal images of sections from tumors stained with CD31 and pericyte marker NG2 ($n = 8$ to 10) and quantification of total NG2-positive signal (*C*) ($n = 4$ to 5 per group). *P* values were determined by a two-tailed unpaired Mann–Whitney test comparing control *S1pr2* WT and *S1pr2* ECKO mice. (*D*) Lung colonization of B16F10 cells injected i.v. in *S1pr2* WT and ECKO mice. The image is representative of three independent experiments. (*E*) Quantification of metastatic foci is expressed as mean ± SD. *P* values were determined by a two-tailed unpaired *t* test with Welch's comparing control and *S1pr2* ECKO mice. (*F*) Whole-tumor weight of s.c. LLC tumors grown in *S1pr1*, *S1pr2* WT and ECKO mice. $n = 3$ independent experiments containing three mice per group, expressed as a mean of two tumors per animal ± SD. *P* values were determined by a two-tailed unpaired Mann–Whitney *U* test comparing *S1pr1*, *S1pr2* WT and ECKO mice. (*G*) Whole-tumor weight of s.c. LLC tumors grown in *S1pr1* WT, *S1pr3*$^{-/-}$ and *S1pr1* ECKO, *S1pr3*$^{-/-}$ mice. $n = 2$ independent experiments containing three or four mice per group, expressed as a mean of two tumors per animal ± SD. (*H*) Whole-tumor weight of s.c. LLC tumors grown in *S1pr1* WT, *S1pr2* WT, *S1pr3*$^{-/-}$ and *S1pr1* ECKO, *S1pr2* ECKO, *S1pr3*$^{-/-}$ mice. $n = 2$ independent experiments containing two or three mice per group, expressed as a mean of two tumors per animal ± SD. *P* values were determined by a two-tailed unpaired Mann–Whitney *U* test comparing *S1pr3*$^{-/-}$ and *S1pr1* ECKO, *S1pr2* ECKO, *S1pr3*$^{-/-}$ mice. (*I*) The 35 µm tumor sections stained with CD31, α-SMA, and NG2 antibodies show vascular morphology and mural cell coverage. ns, nonsignificant; $*P \leq 0.05$, $**P \leq 0.01$, $***P \leq 0.001$.

progression in numerous murine models (28, 29). However, in some tumors, modulation of myeloid phenotypes by specific activation of the CD11b integrin molecule leads to a myeloid phenotype switch and responsiveness to antitumor therapy (49). In addition, a reduced number of DCs could attenuate antitumor immunity via the adaptive immune system (27, 50). Such mechanisms may lead to enhanced tumor growth in *S1pr1* ECKO mice. We speculate that elaboration of angiocrine functions of tumor endothelial cells may influence myeloid cell content of the TME.

In addition, we show that the signaling of endothelial S1PR1 influences the ability of circulating tumor cells to establish metastatic colonies in the lungs. Since defective endothelial junctions leading to decreased barrier properties of the tumor vessels are controlled by this receptor, we suggest that this function of the S1P signaling

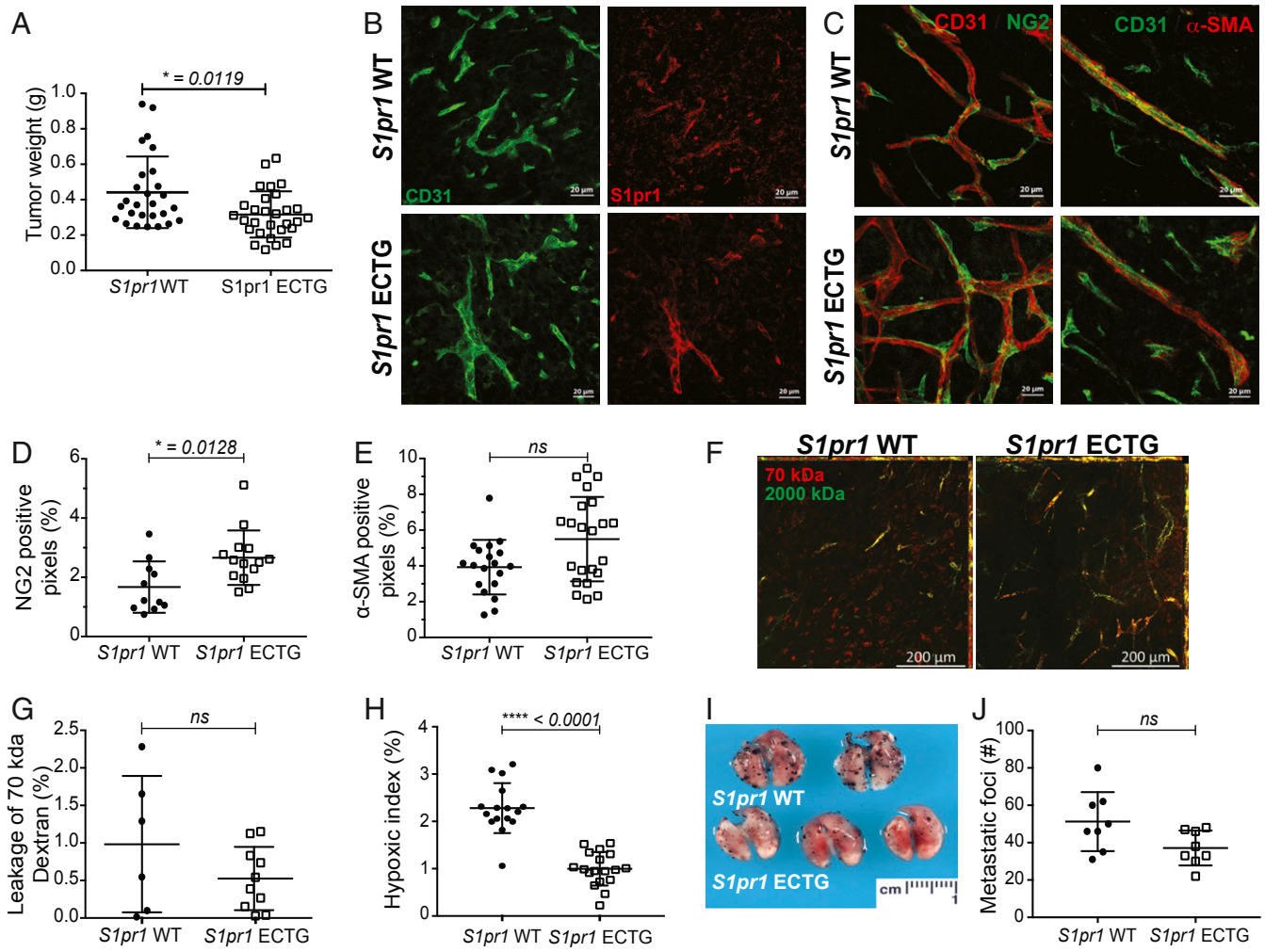

Fig. 5. Overexpression of EC-specific S1PR1 enhances mural cell coverage, and reduces tumor growth, vascular leakage, and metastasis. (*A*) Whole-tumor weight of s.c. LLC tumors grown in control *S1pr1* WT and ECTG mice. $n = 7$ independent experiments containing three or four mice per group, expressed as a mean of two tumors per animal ± SD. (*B*) Confocal microscopy images of 35 μm sections of tumor, stained with S1PR1 and CD31 antibodies, show induced expression of S1PR1 in endothelial cells and vessel morphology. Quantification of NG2 (*C*) and α-SMA (*D*) positive pixels from confocal images ($n = 11$ to 22) of 35 μm sections of tumor sections from *S1pr1* WT and ECTG mice and stained with NG2 or α-SMA and CD31 antibodies (*E*). Data are expressed as mean ± SD. (*F*) Quantification of extravasated 70 kDa dextran ($n = 6$ to 10 per group) from confocal images of 35 μm tumors sections grown in *S1pr1* WT and ECTG mice, i.v. injected with 2,000 kDa (fluorescein, green) and 70 kDa (tetramethylrhodamine-conjugated dextran [TMR], red) dextran. $n = 2$ independent experiments containing three or four mice per group (*G*). Data are expressed as mean ± SD. (*H*) Quantification of Hypoxyprobe-1 staining images ($n = 2$ independent experiment, and three to four images were quantified per group per experiment). (*I*) Lung colonization of B16F10 cells injected i.v. in *S1pr1* WT and ECTG mice. Image is representative of three independent experiments. (*J*) Quantification of metastatic foci. Data are expressed as mean ± SD. *P* values were determined by a two-tailed unpaired Mann–Whitney *U* test comparing control and *S1pr1* ECTG mice. ns, nonsignificant; $*P \leq 0.05$, $****P \leq 0.0001$.

axis regulates the metastatic potential of circulating tumor cells. However, endothelial S1PR1 regulation of myeloid populations in the TME and the elaboration of antitumor immunity may also be involved. In fact, it was recently shown that loss of the S1P transporter Spns2, which is highly expressed in the endothelium, suppressed the metastatic potential of circulating tumor cells in mouse models (51).

Using the genetic loss of function models of S1PR2 and S1PR3, either alone or in combination with S1PR1, we show that these two S1PRs compensate for the loss of S1PR1 in tumor vascular endothelium. This finding may be useful in the design of therapeutic approaches to enhance tumor vascular normalization. For example, genetic and/or pharmacological approaches to enhance tumor endothelial S1PR1 signaling may induce tumor vascular normalization.

We also demonstrate that the S1PR1-induced tumor vascular normalization pathway is functionally relevant because both chemotherapy (doxorubicin) and immunotherapy (anti-PD-1 antibody) were significantly more effective in suppression of tumor growth in endothelial S1PR1 transgenic mice. Further studies to refine this finding may lead to novel therapeutic approaches in solid tumors.

In summary, our study shows that endothelial S1PR signaling is an important factor in tumor vascular phenotype that influences tumor progression, metastasis, and chemo- and immunotherapeutic efficacy of preclinical mouse tumor models. Strategies to enhance S1PR1 function in the tumor vasculature may potentiate the efficacy of cytotoxic and targeted anticancer therapies.

Materials and Methods

Mouse Strains. Mice were housed in a temperature-controlled facility with a 12 h light/dark cycle, specific pathogen free, in individual ventilated cages and were provided food and water ad libitum. All animal experiments were approved by the Boston Children's Hospital and Weill Cornell Medicine

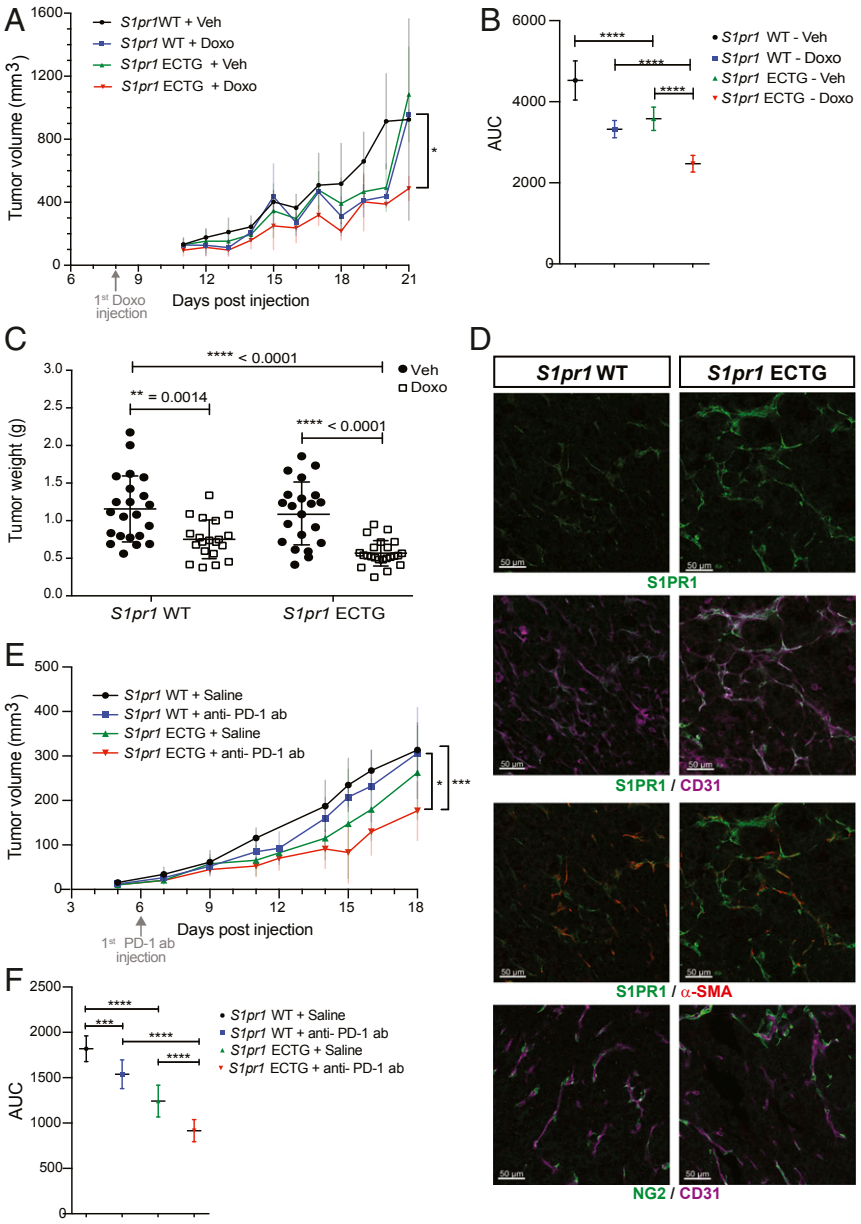

Fig. 6. Vascular normalization induced by endothelial S1PR1 potentiates the effect of antitumor agents. s.c. LLCs and syngeneic breast cancer model cells (E0771 cells) were grown in *S1pr1* WT and ECTG and were subjected to specific antitumor agents. (*A*) LLC tumor–bearing mice were treated with 5 mg/kg of doxorubicin or vehicle starting at day 8, and the volume presented was measured every day until harvest. $n = 8$ independent experiments each containing three or four mice per group, expressed as a mean of two tumors per animal ± SD. *P* values were determined by a two-way ANOVA mixed-effects analysis (restricted maximum likelihood [REML] method) multiple comparisons test comparing *S1pr1* WT and ECTG mice ± doxorubicin. $*P \leq 0.05$ between WT and ECTG mice treated with doxorubicin at day 21. (*B*) Area under the curve (AUC) for each condition presented in *A*. *P* values were determined by a one-way ANOVA multiple comparisons test comparing *S1pr1* WT and ECTG mice ± doxorubicin. $****P \leq 0.0001$. (*C*) Whole-tumor weight of s.c. LLC tumors grown in *S1pr1* WT and ECTG mice at harvest time, treated with 5 mg/kg of doxorubicin or vehicle. $n = 8$ independent experiments each containing three or four mice per group, expressed as a mean of two tumors per animal ± SD. *P* values were determined by two-way ANOVA followed by Sidak's multiple comparisons test comparing *S1pr1* WT and ECTG mice ± doxorubicin. $**P \leq 0.01$, $****P \leq 0.0001$. (*D*) Immunofluorescence of 25 μm sections of frozen E0771 tumors from S1pr1 WT and ECTG mice, stained with S1PR1, α-SMA, CD31, and NG2 antibodies. (*E*) E0771 tumor-bearing mice were treated with 10 mg/kg of anti-PD-1 antibody or saline, starting at day 6 after injection, and the volume presented was measured every other day until harvest. $n = 4$ independent experiments each containing two to four mice per group, expressed as a mean of four tumors per animal ± SD. *P* values were determined by a two-way ANOVA mixed-effects analysis (REML) multiple comparisons test comparing *S1pr1* WT and ECTG mice ± anti-PD-1 antibody. $*P \leq 0.05$ between WT and ECTG mice treated with anti-PD-1 on days 11, 14, and 16; $***P \leq 0.001$ between WT+saline and ECTG+PD-1 mice on day 11. (*F*) Area under the curve for each condition presented in *E*. $***P \leq 0.001$, $****P \leq 0.0001$.

Institutional Animal Care and Use Committees. EC-specific *S1pr1* knockout mice (*S1pr1*$^{f/f}$ Cdh5-Cre-ER^{T2}; *S1pr1* ECKO) were generated as described (5, 21–23). EC-specific *S1pr2* knockout mice (*S1pr2*$^{f/f}$ Cdh5-Cre-ER^{T2}; *S1pr2* ECKO) were generated as described in *SI Appendix, Material and Methods*. EC-specific *S1pr1-S1pr2* double-knockout mice were generated by crossing *S1pr1* ECKO with *S1pr2* ECKO mice. EC-specific *S1pr1-S1pr2* double-knockout mice in the *S1pr3*$^{-/-}$ background were generated by crossing the *S1pr1* ECKO–*S1pr2* ECKO mice with *S1pr3*$^{-/-}$ mice (7). *S1pr1*$^{fl/stop/f}$ was generated as described (5, 21) by knocking the transgene into embryonic stem cells (ESCs) and crossed with Cdh5-Cre-ER^{T2} mice. Gene deletion or overexpression by the cre recombinase was achieved by intraperitoneal (i.p.) injection of tamoxifen (Sigma-Aldrich) (150 μg/g body weight per day) at 6 wk of age for five consecutive days, and

mice were allowed to recover for 2 wk before being used for experiments. Littermates without the Cdh5–Cre–ER^{T2} gene were treated with tamoxifen in the same way and used as controls. S1P1-GFP signaling reporter mice were previously described (20). Mice expressing one allele of both transgenes were considered S1PR1-GFP signaling mice. Littermates expressing only the H2B-GFP allele without the S1PR1 knock-in were considered controls (20). All genotyping was done by PCR using ear punch biopsies.

Cell Lines. LLCs (ATCC-CRL-1642) used for s.c. injection and B16F10 cells (ATCC-CRL-6475) used for metastasis were grown in Dulbecco's modified Eagle medium (DMEM) supplemented with 10% heat-inactivated fetal bovine serum (FBS). Mouse breast adenocarcinoma cells E0771 (CH3 BioSystems) were grown in RPMI 1640 supplemented with 10 mmol/L Hepes and 10% FBS. All cell lines were tested with the IMPACTIII Rodent Pathogen Testing (IDEXX RADIL, University of Missouri) prior to experiments in mice.

Tumor Growth, Volume, and Drug Administration. LLCs (5×10^5 suspended in Hank's Balanced Salt Solution [HBSS]) were injected s.c. on both flanks into the indicated mice. Sixteen days later, tumors were harvested and analyzed further. For water content, tumors were weighed following harvest, dried overnight in a 60° oven, and weighed again. Percent water content was calculated using the formula $-((\text{wet weight} - \text{dry weight})/\text{wet weight}) \times 100$. Doxorubicin (Sigma-Aldrich) was administered at a final dose of 5 mg/kg body weight via i.p. injection every other day, starting 8 d after tumor cell injection. Control animals were treated with the vehicle, HBSS. Tumor-bearing mice were killed 22 d after LLC injection. B16F10 cells (10^6 in HBSS) were injected i.v. in the tail vein into the indicated mice. Twenty days later, mice were killed by CO_2 and perfused with 10 mL of PBS, and lungs were harvested. Metastatic foci in lung tissue sections were counted under a microscope. Murine breast adenocarcinoma (E0771) cells (2×10^5 suspended in HBSS) were injected in the third (under the front leg) and fourth (above the hind leg) mammary fat pads, on both sides, of *S1pr1* WT and ECTG mice. Anti-PD-1 antibody (BioXcell, clone RMP1-14, CD279) was administered at a final dose of 10 mg/kg body weight via i.p. injection every 3 d, starting 6 d after tumor cell injection, when tumors were palpable. Control animals were treated with saline. Tumor-bearing mice were killed 18 d after injection, when the tumor volume reached almost 500 mm^3. Tumors (LLC and E0771) were measured with calipers daily or every other day, and tumor volume was calculated as $((d^2 \times D) \times \pi)/6$, where d = inner diameter, D = outer diameter, and $\pi = 3.1416$.

Immunostaining, Imaging, and Quantification. Freshly harvested tumors were fixed and embedded in optimal cutting temperature (OCT) or paraffin. Sections were stained, and images were acquired by confocal or light microscopy and used for further quantifications. (See details in *SI Appendix, Material and Methods*.)

Tumor Vessel Leakiness. Tumor-bearing mice were injected with two different molecular-size dextran (70 and 2000 kDa), and vessel leakiness in tumor sections was quantified as described in *SI Appendix, Material and Methods*.

Quantitation of Tumor Hypoxia. Tumor-bearing mice were injected with Hypoxyprobe-1, and tumor sections were stained with Hypoxyprobe-1 antibody; the hypoxic index was quantified as described in *SI Appendix, Material and Methods*.

TME Immune Cell Population Flow Cytometry Analysis. LLC tumors were harvested, digested to a single-cell suspension, and stained for different immune cell markers. Tumor immune cell populations were analyzed by flow cytometry and FlowJo software. (See details in *SI Appendix, Material and Methods*.)

Statistical Analysis. Statistical analysis was performed using GraphPad Prism software, version 8.2. A two-tailed unpaired Mann–Whitney *U* test or *t* test with Welch's correction was used for direct comparison of two groups. ANOVA followed by Sydak's multiple comparisons test to compare all groups was used to determine significance between three or more test groups. Mixed-effects analysis with multiple comparisons was used to compare tumor volume curves between four groups. All values reported are means ± SD. All animal experiments used randomization to treatment groups and blinded assessment.

Data Availability. Raw images of tumor vascular analysis and tumor growth (Excel files) have been analyzed for qualitative and quantitative representation in the figures and the supplemental materials. Original images and Excel files may be obtained from the corresponding author upon request.

ACKNOWLEDGMENTS. The authors thank Dr. Rakesh Jain for advice on immunotherapy experiments, Dr. Diane Bielenberg and Dr. Bruce Zetter for advice on metastatic experiments, Dr. David Zurakowski for biostatistics advice, and Kristin Johnson for graphics assistance. This work was supported by NIH Grants HL89934, HL117798, and R35 HL135821 (to T.H.); a Leducq Foundation Transatlantic Network Grant (SphingoNet; to T.H.); and a postdoctoral fellowship from the American Heart Association 18POST33990452 (to A.C.). The flow cytometry experiments were performed at the Department of Hematology/Oncology Flow Cytometry Research Facility at Boston Children's Hospital, which is supported by NIH Grant U54DK110805-03 and the Harvard Stem Cell Institute.

1. A. Cartier, T. Hla, Sphingosine 1-phosphate: Lipid signaling in pathology and therapy. *Science* **366**, eaar5551 (2019).
2. R. L. Proia, T. Hla, Emerging biology of sphingosine-1-phosphate: Its role in pathogenesis and therapy. *J. Clin. Invest.* **125**, 1379–1387 (2015).
3. Y. Liu *et al*., Edg-1, the G protein-coupled receptor for sphingosine-1-phosphate, is essential for vascular maturation. *J. Clin. Invest.* **106**, 951–961 (2000).
4. J. H. Paik *et al*., Sphingosine 1-phosphate receptor regulation of N-cadherin mediates vascular stabilization. *Genes Dev.* **18**, 2392–2403 (2004).
5. B. Jung *et al*., Flow-regulated endothelial S1P receptor-1 signaling sustains vascular development. *Dev. Cell* **23**, 600–610 (2012).
6. K. Gaengel *et al*., The sphingosine-1-phosphate receptor S1PR1 restricts sprouting angiogenesis by regulating the interplay between VE-cadherin and VEGFR2. *Dev. Cell* **23**, 587–599 (2012).
7. M. Kono *et al*., The sphingosine-1-phosphate receptors S1P1, S1P2, and S1P3 function coordinately during embryonic angiogenesis. *J. Biol. Chem.* **279**, 29367–29373 (2004).
8. K. Mizugishi *et al*., Essential role for sphingosine kinases in neural and vascular development. *Mol. Cell. Biol.* **25**, 11113–11121 (2005).
9. Y. Xiong, P. Yang, R. L. Proia, T. Hla, Erythrocyte-derived sphingosine 1-phosphate is essential for vascular development. *J. Clin. Invest.* **124**, 4823–4828 (2014).
10. J. Folkman, Angiogenesis: An organizing principle for drug discovery? *Nat. Rev. Drug Discov.* **6**, 273–286 (2007).
11. N. Ferrara, Pathways mediating VEGF-independent tumor angiogenesis. *Cytokine Growth Factor Rev.* **21**, 21–26 (2010).
12. P. Carmeliet, R. K. Jain, Principles and mechanisms of vessel normalization for cancer and other angiogenic diseases. *Nat. Rev. Drug Discov.* **10**, 417–427 (2011).
13. R. K. Jain, Normalization of tumor vasculature: An emerging concept in antiangiogenic therapy. *Science* **307**, 58–62 (2005).
14. Y. Huang, S. Goel, D. G. Duda, D. Fukumura, R. K. Jain, Vascular normalization as an emerging strategy to enhance cancer immunotherapy. *Cancer Res.* **73**, 2943–2948 (2013).
15. S. Goel *et al*., Normalization of the vasculature for treatment of cancer and other diseases. *Physiol. Rev.* **91**, 1071–1121 (2011).
16. S. S. Chae, J. H. Paik, H. Furneaux, T. Hla, Requirement for sphingosine 1-phosphate receptor-1 in tumor angiogenesis demonstrated by in vivo RNA interference. *J. Clin. Invest.* **114**, 1082–1089 (2004).
17. K. LaMontagne *et al*., Antagonism of sphingosine-1-phosphate receptors by FTY720 inhibits angiogenesis and tumor vascularization. *Cancer Res.* **66**, 221–231 (2006).
18. H. Azuma *et al*., Marked prevention of tumor growth and metastasis by a novel immunosuppressive agent, FTY720, in mouse breast cancer models. *Cancer Res.* **62**, 1410–1419 (2002).
19. A. S. Fischl *et al*., Inhibition of sphingosine phosphate receptor 1 signaling enhances the efficacy of VEGF receptor inhibition. *Mol. Cancer Ther.* **18**, 856–867 (2019).
20. M. Kono *et al*., Sphingosine-1-phosphate receptor 1 reporter mice reveal receptor activation sites in vivo. *J. Clin. Invest.* **124**, 2076–2086 (2014).
21. V. A. Blaho *et al*., HDL-bound sphingosine-1-phosphate restrains lymphopoiesis and neuroinflammation. *Nature* **523**, 342–346 (2015).
22. S. Galvani *et al*., HDL-bound sphingosine 1-phosphate acts as a biased agonist for the endothelial cell receptor S1P1 to limit vascular inflammation. *Sci. Signal.* **8**, ra79 (2015).
23. K. Yanagida *et al*., Size-selective opening of the blood-brain barrier by targeting endothelial sphingosine 1-phosphate receptor 1. *Proc. Natl. Acad. Sci. U.S.A.* **114**, 4531–4536 (2017).
24. G. Helmlinger, F. Yuan, M. Dellian, R. K. Jain, Interstitial pH and pO2 gradients in solid tumors in vivo: High-resolution measurements reveal a lack of correlation. *Nat. Med.* **3**, 177–182 (1997).
25. J. Chen *et al*., Suppression of retinal neovascularization by erythropoietin siRNA in a mouse model of proliferative retinopathy. *Invest. Ophthalmol. Vis. Sci.* **50**, 1329–1335 (2009).
26. F. R. Balkwill, M. Capasso, T. Hagemann, The tumor microenvironment at a glance. *J. Cell Sci.* **125**, 5591–5596 (2012).
27. J. A. Joyce, D. T. Fearon, T cell exclusion, immune privilege, and the tumor microenvironment. *Science* **348**, 74–80 (2015).
28. F. Klemm, J. A. Joyce, Microenvironmental regulation of therapeutic response in cancer. *Trends Cell Biol.* **25**, 198–213 (2015).

29. D. F. Quail, J. A. Joyce, Microenvironmental regulation of tumor progression and metastasis. *Nat. Med.* **19**, 1423–1437 (2013).
30. M. J. Lee *et al*., Vascular endothelial cell adherens junction assembly and morphogenesis induced by sphingosine-1-phosphate. *Cell* **99**, 301–312 (1999).
31. A. Skoura *et al*., Essential role of sphingosine 1-phosphate receptor 2 in pathological angiogenesis of the mouse retina. *J. Clin. Invest.* **117**, 2506–2516 (2007).
32. T. Sanchez *et al*., Induction of vascular permeability by the sphingosine-1-phosphate receptor-2 (S1P2R) and its downstream effectors ROCK and PTEN. *Arterioscler. Thromb. Vasc. Biol.* **27**, 1312–1318 (2007).
33. M. Adada, D. Canals, Y. A. Hannun, L. M. Obeid, Sphingosine-1-phosphate receptor 2. *FEBS J.* **280**, 6354–6366 (2013).
34. R. T. Windh *et al*., Differential coupling of the sphingosine 1-phosphate receptors Edg-1, Edg-3, and H218/Edg-5 to the G(i), G(q), and G(12) families of heterotrimeric G proteins. *J. Biol. Chem.* **274**, 27351–27358 (1999).
35. T. Hla, Sphingosine 1-phosphate receptors. *Prostaglandins Other Lipid Mediat.* **64**, 135–142 (2001).
36. T. Sanchez, T. Hla, Structural and functional characteristics of S1P receptors. *J. Cell. Biochem.* **92**, 913–922 (2004).
37. Y. Hisano, T. Hla, Bioactive lysolipids in cancer and angiogenesis. *Pharmacol. Ther.* **193**, 91–98 (2019).
38. M. E. Pitulescu, I. Schmidt, R. Benedito, R. H. Adams, Inducible gene targeting in the neonatal vasculature and analysis of retinal angiogenesis in mice. *Nat. Protoc.* **5**, 1518–1534 (2010).
39. G. Minotti, P. Menna, E. Salvatorelli, G. Cairo, L. Gianni, Anthracyclines: Molecular advances and pharmacologic developments in antitumor activity and cardiotoxicity. *Pharmacol. Rev.* **56**, 185–229 (2004).
40. P. K. Singal, N. Iliskovic, Doxorubicin-induced cardiomyopathy. *N. Engl. J. Med.* **339**, 900–905 (1998).
41. S. Wang *et al*., Doxorubicin induces apoptosis in normal and tumor cells via distinctly different mechanisms. intermediacy of H(2)O(2)- and p53-dependent pathways. *J. Biol. Chem.* **279**, 25535–25543 (2004).
42. A. R. Cantelmo *et al*., Inhibition of the glycolytic activator PFKFB3 in endothelium induces tumor vessel normalization, impairs metastasis, and improves chemotherapy. *Cancer Cell* **30**, 968–985 (2016).
43. S. L. Topalian, J. M. Taube, R. A. Anders, D. M. Pardoll, Mechanism-driven biomarkers to guide immune checkpoint blockade in cancer therapy. *Nat. Rev. Cancer* **16**, 275–287 (2016).
44. C. N. Johnstone *et al*., Functional and molecular characterisation of EO771.LMB tumours, a new C57BL/6-mouse-derived model of spontaneously metastatic mammary cancer. *Dis. Model. Mech.* **8**, 237–251 (2015).
45. V. P. Chauhan *et al*., Reprogramming the microenvironment with tumor-selective angiotensin blockers enhances cancer immunotherapy. *Proc. Natl. Acad. Sci. U.S.A.* **116**, 10674–10680 (2019).
46. C. Kasikara *et al*., Pan-TAM tyrosine kinase inhibitor BMS-777607 enhances anti-PD-1 mAb efficacy in a murine model of triple-negative breast cancer. *Cancer Res.* **79**, 2669–2683 (2019).
47. E. J. Crosby *et al*., Complimentary mechanisms of dual checkpoint blockade expand unique T-cell repertoires and activate adaptive anti-tumor immunity in triple-negative breast tumors. *OncoImmunology* **7**, e1421891 (2018).
48. K. Gaengel, G. Genové, A. Armulik, C. Betsholtz, Endothelial-mural cell signaling in vascular development and angiogenesis. *Arterioscler. Thromb. Vasc. Biol.* **29**, 630–638 (2009).
49. R. Z. Panni *et al*., Agonism of CD11b reprograms innate immunity to sensitize pancreatic cancer to immunotherapies. *Sci. Transl. Med.* **11**, eaau9240 (2019).
50. K. Palucka, J. Banchereau, Cancer immunotherapy via dendritic cells. *Nat. Rev. Cancer* **12**, 265–277 (2012).
51. L. van der Weyden *et al*., Genome-wide in vivo screen identifies novel host regulators of metastatic colonization. *Nature* **541**, 233–236 (2017).